

# Conditions for Statistical Determination of the Neutrino Mass Spectrum in Radiative Emission of Neutrino Pairs in Atoms

Ningqiang Song,<sup>1,\*</sup> R. Boyero Garcia,<sup>2,†</sup> J. J. Gomez-Cadenas,<sup>3,‡</sup> M. C. Gonzalez-Garcia,<sup>4,5,1,§</sup> A. Peralta Conde,<sup>2,¶</sup> and Josep Taroni<sup>5,\*\*</sup>

<sup>1</sup>*C.N. Yang Institute for Theoretical Physics, SUNY at Stony Brook, Stony Brook, NY 11794-3840, USA*

<sup>2</sup>*Centro de Láseres Pulsados, CLPU, Parque Científico, 37185 Villamayor, Salamanca, Spain.*

<sup>3</sup>*Instituto de Física Corpuscular (IFIC), CSIC & Universitat de Valencia, Calle Catedrático José Beltrán, 2, 46980 Paterna, Valencia, Spain*

<sup>4</sup>*Institució Catalana de Recerca i Estudis Avançats (ICREA),*

<sup>5</sup>*Departament d'Estructura i Constituents de la Matèria, Universitat de Barcelona, 647 Diagonal, E-08028 Barcelona, Spain*

The photon spectrum in macrocoherent atomic de-excitation via radiative emission of neutrino pairs (RENP) has been proposed as a sensitive probe of the neutrino mass spectrum, capable of competing with conventional neutrino experiments. In this paper we revisit this intriguing technique in order to quantify the requirements for statistical determination of some of the properties of the neutrino spectrum, in particular the neutrino mass scale and the mass ordering. Our results are sobering. We find that, even under ideal conditions, the determination of neutrino parameters needs experimental live times of the order of days to years for several laser frequencies, assuming a target of volume of order 100 cm<sup>3</sup> containing about 10<sup>21</sup> atoms per cubic centimeter in a totally coherent state with maximum value of the electric field in the target. Such conditions seem to be, as of today, way beyond the reach of our current technology.

## I. INTRODUCTION

Neutrino oscillation experiments have now established beyond doubt that neutrinos are massive and there is leptonic flavour violation in their propagation [1, 2] (see [3] for an overview). A consistent description of the global data on neutrino oscillations is possible by assuming that the three known neutrinos ( $\nu_e$ ,  $\nu_\mu$ ,  $\nu_\tau$ ) are linear quantum superposition of three massive states  $\nu_i$  ( $i = 1, 2, 3$ ) with masses  $m_i$ . Consequently, a leptonic mixing matrix is present in the weak charged current interactions [4, 5] of the mass eigenstates, which can be parametrized as [6]:

$$U = \begin{pmatrix} c_{12}c_{13} & s_{12}c_{13} & s_{13}e^{-i\delta_{\text{CP}}} \\ -s_{12}c_{23} - c_{12}s_{13}s_{23}e^{i\delta_{\text{CP}}} & c_{12}c_{23} - s_{12}s_{13}s_{23}e^{i\delta_{\text{CP}}} & c_{13}s_{23} \\ s_{12}s_{23} - c_{12}s_{13}c_{23}e^{i\delta_{\text{CP}}} & -c_{12}s_{23} - s_{12}s_{13}c_{23}e^{i\delta_{\text{CP}}} & c_{13}c_{23} \end{pmatrix} \begin{pmatrix} 1 & 0 & 0 \\ 0 & e^{i\eta_1} & 0 \\ 0 & 0 & e^{i\eta_2} \end{pmatrix} \quad (1)$$

where  $c_{ij} \equiv \cos\theta_{ij}$  and  $s_{ij} \equiv \sin\theta_{ij}$ . The phases  $\eta_i$  are only non-zero if neutrinos are Majorana particles. If one chooses the convention where the angles  $\theta_{ij}$  are taken to lie in the first quadrant,  $\theta_{ij} \in [0, \pi/2]$ , and the CP phases  $\delta_{\text{CP}}, \eta_1, \eta_2 \in [0, 2\pi]$ , then  $\Delta m_{21}^2 = m_2^2 - m_1^2 > 0$  by convention, and  $\Delta m_{31}^2$  can be positive or negative. It is customary to refer to the first option as Normal Ordering (NO), and to the second one as Inverted Ordering (IO).

---

\*Electronic address: ningqiang.song@stonybrook.edu

†Electronic address: robertobg@usal.es

‡Electronic address: gomez@mail.cern.ch,

§Electronic address: maria.gonzalez-garcia@stonybrook.edu

¶Electronic address: aperalta@clpu.es

\*\*Electronic address: taron@ecm.ub.edu

At present the global analysis of neutrino oscillation data yields the three-sigma ranges for the parameters [7]

	$3\sigma$ range	
$\sin^2 \theta_{12}$	$0.270 \rightarrow 0.344$	
$\sin^2 \theta_{23}$	$0.385 \rightarrow 0.644$	
$\sin^2 \theta_{13}$	$0.0188 \rightarrow 0.0251$	
$\delta_{\text{CP}}/^\circ$	$0 \rightarrow 360$	,
$\frac{\Delta m_{21}^2}{10^{-5} \text{ eV}^2}$	$7.02 \rightarrow 8.09$	
$\frac{\Delta m_{3\ell}^2}{10^{-3} \text{ eV}^2}$	$\begin{bmatrix} +2.325 \rightarrow +2.599 \\ -2.590 \rightarrow -2.307 \end{bmatrix}$	

but gives no information on the Majorana phases nor on the Dirac or Majorana nature of the neutrino. They do not provide a measurement of the absolute neutrino masses as well, but only of their differences. In the table  $\Delta m_{3\ell}^2$  corresponds to the largest mass splitting (in absolute value) with  $\ell = 1$  for NO and  $\ell = 2$  for IO. As seen from the table, at present, oscillation experiments have not provided us with information of the ordering either.

The determination of the ordering and the CP violating phase  $\delta_{\text{CP}}$  is the main goal of ongoing long baseline (LBL) oscillation experiments [8–10] which are sensitive to those in some part of the parameter space. Definite knowledge is better guaranteed in future projects [11, 12].

Concerning the determination of the absolute mass scale in laboratory experiments, the standard approach is the search for the distortion of the end point of the electron spectrum in tritium beta decay. At present the most precise experiments [13, 14] have given no indication in favor of distortion what sets an upper limit

$$m_{\nu_e} = \left[ \sum_i m_i^2 |U_{ei}|^2 \right]^{1/2} < 2.2 \text{ eV} . \quad (3)$$

The ongoing KATRIN experiment [15], is expected to achieve an estimated sensitivity limit:  $m_\beta \sim 0.3 \text{ eV}$ .

The most precise probe of the nature of the neutrino is the search of neutrino-less double beta decay for verification of lepton number violation which is related to neutrino Majorana masses (for a recent review see Ref. [16]). So far this decay has not been observed and the strongest bounds arise from experiments using  $^{76}\text{Ge}$  [17],  $^{136}\text{Xe}$  [18, 19], and  $^{130}\text{Te}$  [20]. For the case in which the only effective lepton number violation at low energies is induced by the Majorana mass term for the neutrinos, the rate of  $0\nu\beta\beta$  decay is proportional to the *effective Majorana mass* of  $\nu_e$ , and the experimental bounds on the corresponding lifetimes can be translated in constraints on the combination

$$m_{ee} = \left| \sum_i m_i U_{ei}^2 \right| \lesssim 0.14 \rightarrow 0.76 \text{ eV} , \quad (4)$$

which, in addition to the masses and mixing parameters that affect the tritium beta decay spectrum, depends also on two combinations of the CP violating phases  $\delta_{\text{CP}}$  and  $\eta_i$ .

An unexpected new way to explore fundamental neutrino physics may come from the field of quantum optics, thanks to recent technological advances. The key concept behind the intriguing possibility is the small energy difference between the levels in the atom or molecule, which allows for large relative effects associated with the small neutrino masses in the energy released in level transitions. This, in turn, opens up the possibility of precision neutrino mass spectroscopy, as proposed by Ref. [21–23].

The relevant process in this case is the atomic de-excitation via radiative emission of neutrino pairs (RENP):  $|e\rangle \rightarrow |g\rangle + \gamma + \nu_i \bar{\nu}_j$ . The rate of this process can be made measurable if macro-coherence of the atomic target can be achieved [22, 24]. The proposal is to reach such macro-coherent emission of radiative neutrino pairs via stimulation by irradiation of two trigger lasers of frequencies  $\omega, \omega'$  constrained by  $\omega + \omega' = \epsilon_{eg}/\hbar, \omega < \omega'$ , with  $E_{eg} = E_e - E_g$  being the energy difference of initial and final levels. With this set-up the energy of the emitted photon in the de-excitation is given by the smaller laser frequency  $\omega$  and therefore it can be very precisely known. Furthermore, neglecting atomic recoil, energy-momentum conservation implies that each time the energy of the emitted photon decreases below  $\omega_{ij}$  with

$$\omega_{ij} = \frac{E_{eg}}{2} - \frac{(m_i + m_j)^2}{2E_{eg}} \quad (5)$$

a new channel (this is, emission of another pair of massive neutrino species) is kinematically open.

Location of these threshold energies, by changing the laser frequency is, in principle possible, since the laser frequency, and therefore the emitted photon energy, is known to high precision. Consequently once the six  $\omega_{ij}$  are measured, the spectrum of the neutrino masses could be fully identified. It has been argued that this method is ultimately capable of determining the neutrino mass scale, the mass ordering, the Dirac vs Majorana nature, as well as of measuring the Majorana CP violating phases [21–23].

In this article we revisit this proposal with the aim at quantifying the requirements for statistical determination of some of these properties of the neutrino spectrum, in particular the neutrino mass scale and the mass ordering. To do so we will review in Sec. II the derivation of the rate for RENP and the corresponding photon energy spectrum. Section III contains our quantitative results and conclusions.

## II. PHOTON ENERGY RATE IN RENP AND NEUTRINO SPECTRUM

The expected rate for RENP and the energy spectrum of the emitted photon has been derived in Refs. [22, 23] and we have reproduced it (up to an overall factor 4). For the sake of completeness we summarize here the main elements and assumptions entering the derivation.

The starting point is the effective Hamiltonian describing the atomic transition  $|e\rangle \rightarrow |g\rangle + \gamma + \nu_i \bar{\nu}_j$  assuming that the process cannot proceed directly but only via an intermediate *virtual* state  $|p\rangle$  with  $E_p > E_e > E_g$ , and that the transition between  $|p\rangle$  and  $|g\rangle$  is of type E1 and leads to the emission of the photon while the transition between  $|e\rangle$  and  $|p\rangle$  is of type M1 leading to the emission of the neutrino pair. In this case, after integrating out the intermediate state  $|p\rangle$  in the Markovian and slow varying envelope approximation (see appendix A in [24]), the Schroedinger equation for the effective two-level atomic system state,  $|\psi(x, t)\rangle = c_e(x, t)|e\rangle + c_g(x, t)|g\rangle$ ,

$$\frac{d}{dt}\psi(x, t) \equiv \frac{d}{dt} \begin{pmatrix} c_e(x, t) \\ c_g(x, t) \end{pmatrix} = -i H_{\text{RENP}}(x, t) \begin{pmatrix} c_e(x, t) \\ c_g(x, t) \end{pmatrix}, \quad (6)$$

where  $H_{\text{RENP}}(x, t)$  takes the matrix form

$$H_{\text{RENP}}(x, t) = H_{eg}^R(x, t) \frac{\sigma_1 - i\sigma_2}{2}, \quad (7)$$

here  $\sigma_i$  are the Pauli matrices, and

$$H_{eg}^R = -\frac{G_F}{\sqrt{2}} \vec{d}_{gp} \cdot \vec{\tilde{E}}^*(x, t) \frac{1}{E + E' + E_{pe}} [\bar{u}_i^\lambda(p) \gamma_\mu (1 - \gamma_5) v_j^{\lambda'}(p')] (v_{ij} J_{V,pe}^\mu - a_{ij} J_{A,pe}^\mu) \exp^{i(\omega + E + E' - E_{eg})t} \exp^{-i(\vec{p} + \vec{p}' + \vec{k})\vec{x}}. \quad (8)$$

$\vec{\tilde{E}}^*(x, t)$  is the amplitude of the electric field, while  $(\omega, \vec{k})$  is the four momentum of the photon. Implicit in this expression is the hypothesis that the RENP transition is driven by two lasers, one of which must have the frequency and wave number of the emitted photon (more below).  $E_{ab} = E_a - E_b$  is the energy difference between two of the atomic levels, and

$$\langle g | \vec{d} | p \rangle = \vec{d}_{gp}, \quad \langle p | \bar{f}_e(x) \gamma^\mu (\gamma^5) f_e(x') | e \rangle = \delta^3(x - x') J_{V(A),pe}^\mu \quad (9)$$

$$v_{ij} = U_{ei}^* U_{ej} - \delta_{ij} \left( \frac{1}{2} - 2 \sin^2 \theta_w \right) \quad a_{ij} = U_{ei}^* U_{ej} - \frac{1}{2} \delta_{ij}. \quad (10)$$

$\vec{d}$  is the electric dipole moment operator, and  $f_e$  is the electron field. In defining the electron atomic currents,  $J_{V(A)}^\mu$ , we have implicitly assumed that the spatial atomic wave function is concentrated around the atomic position  $\vec{x}$  so we have approximated it as a delta function. In the non-relativistic limit for the electron field it can be shown that  $J_V^\mu = 0 = J_A^0$  while  $\vec{J}_{A,pe} = \langle p | 2\vec{S} | e \rangle$ , where  $\vec{S}$  is the spin operator.

For a single atom at position  $\vec{x}_a$  at time  $t$  the transition amplitude from an initial atomic state of wave function  $\psi_f^a(x_a)$  to a final atomic state  $\psi_i^a(x_a)$  at first order in perturbation theory is

$$\begin{aligned} A^a &= \int_{-\infty}^{\infty} H_{eg}^R(x_a, t') dt' \\ &\simeq -\frac{G_F}{\sqrt{2}} \vec{d}_{gp} \cdot \vec{\tilde{E}}^*(x_a, t) \frac{1}{\omega - E_{pg}} [\bar{u}_i^\lambda(p) \gamma_\mu (1 - \gamma_5) v_j^{\lambda'}(p')] a_{ij} J_{A,pe}^\mu \left[ (\psi_f^a(x_a))^\dagger \frac{\sigma_1 - i\sigma_2}{2} \psi_i^a(x_a) \right] \\ &\quad \times \exp^{-i(\vec{p} + \vec{p}' + \vec{k})\vec{x}_a} (2\pi) \delta(E + E' + \omega - E_{eg}). \end{aligned} \quad (11)$$

where the energy momentum conservation condition implies  $E + E' + E_{pe} = E_{pg} - \omega$ , and it is assumed that the time scale for the transition is much shorter than the characteristic time variation of the electric field amplitude. We have introduced the atomic Bloch vector  $\vec{r}^a(x_a, t)$  as:

$$\left[ (\psi_f^a(x_a))^\dagger \frac{\sigma_1 - i\sigma_2}{2} \psi_i^a(x_a) \right] = c_e^a(x_a, t_i) [c_g^a(x_a, t_f)]^* \equiv \frac{r_1^a(x_a, t) - ir_2^a(x_a, t)}{2} \quad (12)$$

The expression above is valid for emission from a single atom. For an ensemble of atoms in a volume  $V$  centered in  $\vec{x}$ , the amplitude is the superposition of the contribution of the  $N$  atoms in the volume. Following Ref. [22] one can approximate the summation as  $\sum_a \exp^{-i(\vec{p}+\vec{p}'+\vec{k})\vec{x}_a} \simeq \frac{N}{V} \int dV \exp^{-i(\vec{p}+\vec{p}'+\vec{k})\vec{x}_a} \rightarrow N/V (2\pi)^3 \delta(\vec{p}+\vec{p}'+\vec{k})$ . In this limit

$$\sum_a A^a = \mathcal{M}(x, t) (2\pi)^4 \delta(E + E' + \omega - E_{eg}) \delta(\vec{p} + \vec{p}' + \vec{k}) \quad (13)$$

where

$$\mathcal{M}(x, t) = -\frac{G_F}{\sqrt{2}} \vec{d}_{gp} \cdot \vec{E}^*(x, t) \frac{1}{\omega - E_{pg}} [\bar{u}_i(p) \gamma_\mu (1 - \gamma_5) v_j(p')] a_{ij} J_{A,pe}^\mu \frac{R_1(x) - iR_2(x)}{2} \quad (14)$$

with the definition

$$\sum_a [r_1^a(x_a, t) - ir_2^a(x_a, t)] \exp^{-i(\vec{p}+\vec{p}'+\vec{k})\vec{x}_a} \equiv [R_1(x, t) - iR_2(x, t)] (2\pi)^3 \delta(\vec{p}+\vec{p}'+\vec{k}) \equiv n(x) [r_1(x, t) - ir_1(x, t)] , \quad (15)$$

where  $\vec{R}$  is the vector characterizing the medium ‘‘polarization’’,  $n(x) = N/V$  is the local density of the medium, so  $\vec{r}(x, t)$  is the mean value of  $\vec{R}$  per atom.

As mentioned above the set-up to stimulate RENP is to radiate the atomic medium (the target) with two counter-propagating trigger lasers of frequencies  $\omega_1$  and  $\omega_2$  which verify  $\omega_1 + \omega_2 = E_{eg}$ , so the emitted photon has  $\omega = \omega_1$  and it is emitted in the direction of laser,  $\vec{k} = \vec{k}_1$ , with  $|\vec{k}_1| = \omega_1$ . Furthermore energy-momentum conservation implies  $E + E' = \omega_2$  and  $\vec{k}_1 = -(\vec{p} + \vec{p}')$ , thus consequently for massive neutrinos  $\omega_1 < \omega_2$ .

The number of stimulated transitions (ie the number of single photons of frequency  $\omega$  emitted recoiling against the undetected neutrinos) per unit time and unit volume is

$$\frac{dN_\gamma(\omega)}{dt d^3x} = \frac{1}{2J_e + 1} \sum_{m_e} \sum_{m_p} \sum_{m_g} \sum_{\lambda, \lambda'} \int |\mathcal{M}|^2 \frac{d^3p}{(2\pi)^3 2E} \frac{d^3p'}{(2\pi)^3 2E'} (2\pi)^4 \delta^3(\vec{p} + \vec{p}' + \vec{k}) \delta(E + E' + \omega - E_{eg}) \quad (16)$$

where we denote by  $m_{e,p,g}$  the third component of the angular momentum of the electron in the corresponding atomic states, and we have averaged over the initial angular configurations  $(2J_e + 1)$  and summed over final ones. We have also summed over all possible configurations in the intermediate state  $|p\rangle$ . Assuming isotropy one introduces the atomic spin factor  $C_{ep}$  as,

$$\sum_{m_p} \sum_{m_e} J_{A,pe}^\mu (J_{A,pe}^\nu)^\dagger = \sum_{m_p} \sum_{m_e} 4 \langle p | S^i | e \rangle \langle e | S^j | p \rangle \equiv \frac{4}{3} \delta^{ij} (2J_e + 1) (2J_p + 1) C_{ep} . \quad (17)$$

Altogether

$$\begin{aligned} \frac{dN_\gamma(\omega)}{dt} &= \frac{2G_F^2}{\pi} (2J_p + 1) C_{ep} \int d^3x \left| \vec{d}_{pg} \cdot \vec{E}(x, t) \right|^2 \left| \frac{R_1(x, t) - iR_2(x, t)}{2} \right|^2 I(\omega) \\ &= 6 G_F^2 V_{\text{tar}} n^3 (2J_p + 1) C_{ep} \gamma_{pg} \frac{E_{eg}}{E_{pg}^3} I(\omega) \eta_\omega(t) \\ &= 0.464 \text{ s}^{-1} (2J_p + 1) C_{ep} \left( \frac{V_{\text{tar}}}{10^2 \text{ cm}^3} \right) \left( \frac{n}{10^{21} \text{ cm}^{-3}} \right)^3 \left( \frac{\gamma_{pg}}{10^8 \text{ s}^{-1}} \right) \left( \frac{E_{eg}}{\text{eV}} \right) \left( \frac{\text{eV}}{E_{pg}} \right)^3 I(\omega) \eta_\omega(t) . \end{aligned} \quad (18)$$

In the second equality we have introduced the dimensionless factor

$$\eta_\omega(t) = \frac{1}{V_{\text{tar}}} \int d^3x \frac{|r_1(x, t)|^2 + |r_2(x, t)|^2}{4} \frac{|\vec{E}(x, t)|^2}{n E_{eg}} \simeq \frac{1}{L} \int_0^L dx \frac{|r_1(x, t)|^2 + |r_2(x, t)|^2}{4} \frac{|\vec{E}(x, t)|^2}{n E_{eg}} \quad (19)$$

where the second equality holds for a long thin cylindrical target of total volume  $V_{\text{tar}}$ .  $\eta_\omega(t)$  quantifies how many of the atoms in the target are coherently set in a state characterized by the same value of  $r_i$  and how much the energy density of the electric field in the medium, which is  $\propto |\vec{E}(x, t)|^2$ , approaches the maximum value  $E_{eg} n$ . Both  $\vec{R}$  and  $\vec{\tilde{E}}(x, t)$  have to be obtained independently by solving the coupled Bloch-Maxwell equations for the electromagnetic field in the presence of the atomic medium polarization (see Ref. [22] and references therein). Furthermore we have introduced the spontaneous dipole transition rate  $\gamma_{pg} = E_{pg}^3 |\vec{d}_{pg}|^2 / (3\pi)$  which is experimentally measurable.

$I(\omega)$  is the spectrum function, which (in agreement with Ref. [23]) reads

$$I(\omega) = \frac{1}{(\omega - E_{eg})^2} \sum_{ij} \Delta_{ij}(\omega) [ |a_{ij}|^2 I_{ij}(\omega) - \delta_M m_i m_j \text{Re}(a_{ij})^2 ] \Theta \left( \omega - \frac{E_{eg}}{2} + \frac{(m_i + m_j)^2}{2E_{eg}} \right) \quad (20)$$

$$\Delta_{ij}(\omega) = \frac{[(E_{eg}(E_{eg} - 2\omega) - (m_i + m_j)^2)(E_{eg}(E_{eg} - 2\omega) - (m_i - m_j)^2)]^{1/2}}{E_{eg}(E_{eg} - 2\omega)} \quad (21)$$

$$I_{ij}(\omega) = \frac{1}{3} \left[ E_{eg}(E_{eg} - 2\omega) + \frac{1}{2}\omega^2 - \frac{1}{6}\omega^2 \Delta_{ij}^2(\omega) - \frac{1}{2}(m_i^2 + m_j^2) - \frac{1}{2} \frac{(E_{eg} - \omega)^2}{E_{eg}^2(E_{eg} - 2\omega)^2} (m_i^2 - m_j^2)^2 \right], \quad (22)$$

$$N_\gamma(\omega) = 0.464 \text{ s}^{-1} \frac{T}{s} (2J_p + 1) C_{ep} \left( \frac{V_{\text{tar}}}{10^2 \text{ cm}^3} \right) \left( \frac{n}{10^{21} \text{ cm}^{-3}} \right)^3 \left( \frac{\gamma_{pg}}{10^8 \text{ s}^{-1}} \right) \left( \frac{E_{eg}}{\text{eV}} \right) \left( \frac{\text{eV}}{E_{pg}} \right)^3 I(\omega) \langle \eta_\omega \rangle, \quad (23)$$

where we denote by  $\langle \eta_\omega \rangle$  the time average of  $\eta_\omega(t)$  along the duration of the laser irradiation.

The requirements of the type of atomic transitions for RENP imposes important constraints on the possible target atoms. Two possible atomic candidates have been identified in the literature: Yb and Xe, for which atomic levels with the required quantum numbers exist [25]:

	Xe				Yb			
	Config	Term	$J$	Level(cm <sup>-1</sup> )	Config	Term	$J$	Level(cm <sup>-1</sup> )
$ g\rangle$	$5p^6$	$^1S$	0	0.0000	$4f^{14}(^1S)6s^2$	$^1S$	0	0.0000
$ e\rangle$	$5p^5(^2P_{3/2})6s$	$^2[3/2]^o$	2	67067.547	$4f^{14}(^1S)6s6p$	$^3P^o$	0	17288.439
$ p\rangle$	$5p^5(^2P_{3/2})6s$	$^2[3/2]^o$	1	68045.156	$4f^{14}(^1S)6s6p$	$^3P^o$	1	17992.007
$E_{eg}(\text{eV})$	8.31632				2.14349			
$E_{pg}(\text{eV})$	8.43653				2.23072			
$\gamma_{pg}(10^8 \text{ s}^{-1})$	2.73				0.0115			
$(2J_p + 1)C_{ep}$	2				2			

We plot in Fig 1 the RENP spectral function  $I(\omega)$  for these two nuclei near the end point for three different values of the lightest neutrino mass,  $m_0$ , and for the best fit values of the oscillation parameters in Eq. (2) for both orderings. The spectrum shows the clear dependence of the end-point frequency on  $m_0$  as well as the differences between NO and IO which mainly results in different normalization for both spectra. The curves in the figure correspond to Dirac neutrinos, but the corresponding curves for Majorana neutrinos are practically indistinguishable for those in the figure.

This figure illustrates the potential of RENP to determine the neutrino mass spectrum as well as the main differences between the two nuclei. First because of the larger value of  $E_{eg}$  the resolution in  $\omega$  (the frequency of the trigger laser) required to resolve the threshold positions must be better for Xe than for Yb. On the other hand, because of the larger decay rate  $\gamma_{pg}$  the expected RENP event rate is larger for Xe.

As seen in Eq. (19) the RENP event rate grows as the third power of the number density of atoms in the target, provided that both the amplitude of the electric field in the target acquires a value close to the maximum allowed, and that the medium atomic polarization approaches its macro-coherent value. In what follows we will quantify the final requirement on this product of factors to statistically determine the neutrino mass scale  $m_0$  and the ordering.

### III. RESULTS

#### A. Determination of the Neutrino Mass Scale

We start by building the simplest observable sensitive to the neutrino mass scale, this is to the value of the end-point frequency.

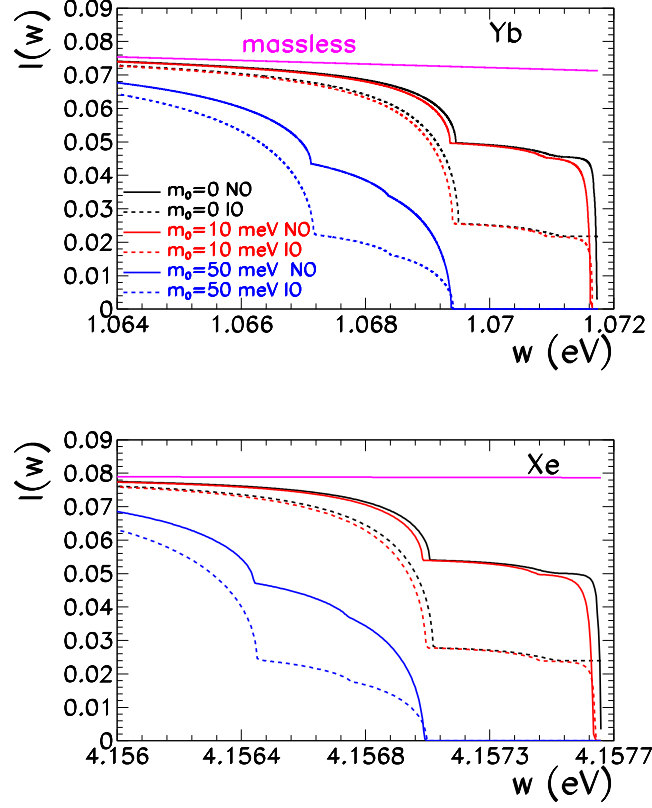


FIG. 1: RENP Spectral function  $I(\omega)$  for Yb (upper panel) and Xe (lower panel) for different values of the lightest neutrino mass  $m_0$  and for both orderings, as labeled in the figure. The curves correspond to the best fit oscillation parameters as given in Eq. (2) and to Dirac neutrinos. The corresponding curves for Majorana neutrinos are practically indistinguishable. For illustration we also show the spectrum for three massless neutrinos.

In order to locate the end-point frequency of the RENP spectrum we foresee a naive experiment starting at a trigger frequency corresponding to the end-point frequency for  $m_0 = 0$ . Clearly no RENP event should be observed at such frequency. One then repeats the experiment lowering one of the laser frequencies (while increasing the other keeping the condition  $\omega_1 + \omega_2 = E_{eg}$ ) in intervals of  $\Delta\omega$  until an observation occurs. If we call  $\omega_+$  to the maximum frequency for which no event is observed and  $\omega_- = \omega_+ - \Delta\omega$  the highest frequency for which some RENP events are observed, the CL at which this naive experiment can determine the neutrino mass scale  $m_0$  with resolution  $\pm\sigma_{m0}$  can be estimated by the conditions

$$N_{\gamma}^{\text{exp}}(\omega_- = \frac{E_{eg}}{2} - 2\frac{[m_0(1 + \sigma_{m0})]^2}{E_{eg}}) = N_{\text{CL}} \quad \text{and} \quad N_{\gamma}^{\text{exp}}(\omega_+ = \frac{E_{eg}}{2} - 2\frac{[m_0(1 - \sigma_{m0})]^2}{E_{eg}}) = 0 \quad (25)$$

where  $N_{\text{CL}}$  is the minimum expected number of events for which at least one event should be observed with a given Confidence Level in Poisson statistics. For example, assuming that our naive experiment is background free we set  $N_{3\sigma} \simeq 5.9$ .

We plot in Fig. 2 the required value of the normalization rate constant

$$N_{\text{norm}} = \left(\frac{T}{s}\right) \left(\frac{V_{\text{tar}}}{10^2 \text{ cm}^3}\right) \left(\frac{n}{10^{21} \text{ cm}^{-3}}\right)^3 \langle \eta_{\omega_0} \rangle, \quad (26)$$

to fulfill condition (25) as a function of  $m_0$  and for different values of  $\sigma_{m0}$ . Notice that in writing Eq. (26) we have neglected the  $\omega$  dependence of the function  $\langle \eta_{\omega} \rangle$  in the range  $\omega_- \geq \omega \geq \omega_+$ . We show the results for an idealized case of perfect knowledge of the laser frequency and for laser with frequency known with finite accuracy  $\sigma_{\text{laser}} = 10^{-5}$  eV, which imposes the additional constraint  $\omega_+ - \omega_- \leq \sigma_{\text{laser}}$ .

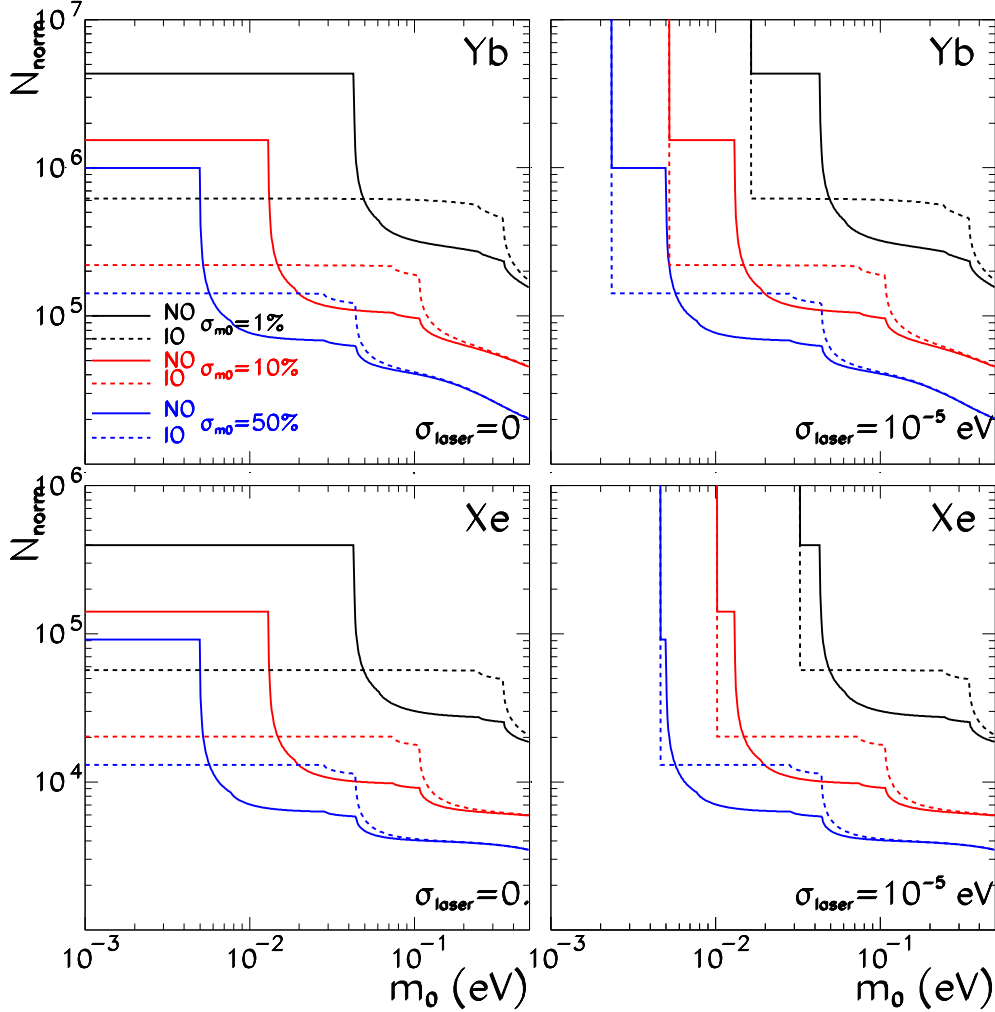


FIG. 2: Required value of the rate normalization factor in Eq.(26) for the location of the end-point frequency of the RENP spectrum with  $3\sigma$  CL leading to a precision in the determination of the corresponding neutrino mass scale of  $m_0 \pm \sigma_{m_0}$  for three values of  $\sigma_{m_0} = 1, 10, 50\%$  (black, red, and blue curves respectively) as a function of  $m_0$ . The full (dashed) lines correspond to NO (IO). The upper (lower) panels are for Yb (Xe) atomic target. In the left panels infinite precision in the knowledge of laser frequency is assumed. In the right panels the laser frequency is assumed to be known with  $10^{-5}$  eV accuracy.

From the figure we see that if the accuracy at which the laser frequency is known was infinite, the required normalization factor would always be lower for Xe as a consequence of the larger decay rate  $\gamma_{pg}$ , even though the level energies involved are larger. The inclusion of a finite accuracy for the laser frequency results in cut-off values  $m_{0,\min}$  below which the determination of  $m_0$  is not possible. They are given by the condition  $\omega_+ - \omega_- \geq \sigma_{\text{laser}}$  and, at a given  $\sigma_{m_0}$ , these maximum reachable values are smaller for Yb than for Xe since the corresponding frequency differences are larger for Yb due to its smaller value of  $E_{eg}$ . We also see that, the required normalization decreases as  $m_0$  increases. This is so despite the overall normalization of  $I(\omega)$  is lower for higher  $m_0$  (see Fig. 1). But the larger is  $m_0$  the larger is the difference between  $\omega_+$  and  $\omega_-$ , so one is sampling the spectrum at lower values, of the frequency, ie further from the final cutoff, where  $I(\omega)$  is relatively larger.

The horizontal asymptotes correspond to values of  $m_0$  for which  $\omega_-$  is above the previous to the last threshold,  $\omega_- > \omega_{12}$  ( $\omega_{31}$ ) for NO (IO), because the spectrum is independent of  $\omega$  in this range. The maximum value of  $m_0$  for which this asymptotic constant rate normalization occurs is independent of the atomic target as it is purely set by the neutrino mass spectrum. It is reached at higher  $m_0$  for IO than for NO since in NO the condition reads  $2m_0(1+\sigma_{m_0}) < (m_1 + m_2)_{\text{NO}} = m_0 + \sqrt{m_0^2 + \Delta m_{21}^2}$  while for IO it is at  $2m_0(1+\sigma_{m_0}) < (m_3 + m_1)_{\text{IO}} = m_0 + \sqrt{m_0^2 + \Delta_{31}^2}$ .

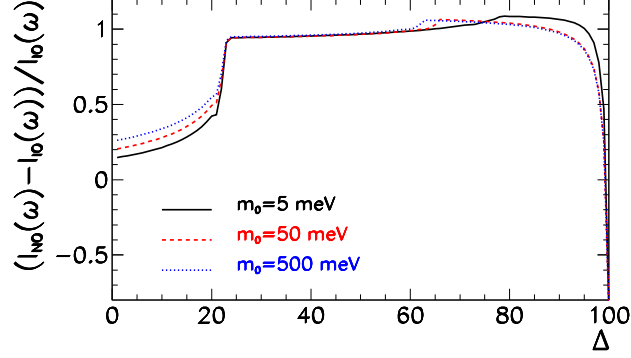


FIG. 3: Relative difference of the RENP spectra for NO and IO as a function of the normalized frequency variable  $\Delta$  defined in Eq. (27) for several values of  $m_0$  as labeled in the figure.

### B. Discrimination between Orderings

Next we consider the minimum requirement for statistical discrimination between the two orderings. We will assume that this is done after the value of  $m_0$  has been established. As seen in Fig. 1 for a given value of  $m_0$  the main difference between the two orderings is the overall normalization with the additional features associated with the different location of the threshold frequencies. To illustrate further the relative size of such features we plot in Fig. 3 the relative difference between the NO and IO RENP spectra for Xe (the corresponding one for Yb is very similar) plotted against a normalized frequency variable:

$$\Delta = 20 + 80 \frac{\omega - \omega_{\min}^{\text{thres}}}{\omega_{\max}^{\text{thres}} - \omega_{\min}^{\text{thres}}}, \quad (27)$$

$$\omega_{\max}^{\text{thres}} = \frac{E_{eg}}{2} - \frac{4m_0^2}{2E_{eg}}, \quad (28)$$

$$\omega_{\min}^{\text{thres}} = \frac{E_{eg}}{2} - \frac{4m_3^2}{2E_{eg}}, \quad \text{with } m_3^2 = m_0^2 + \Delta m_{31}^2 \quad \text{for NO}, \quad (29)$$

$$\omega_{\min}^{\text{thres}} = \frac{E_{eg}}{2} - \frac{4m_2^2}{2E_{eg}}, \quad \text{with } m_2^2 = m_0^2 - \Delta m_{32}^2 \quad \text{for IO}. \quad (30)$$

As seen in the figure there are three main “regions” in the curves, below the lowest threshold, in between the lowest and the previous-to-end point threshold, and above that previous-to-end point threshold. In view of this behaviour we foresee a naive experiment which samples the spectra for three values of the frequency, each one, corresponding to these three regions, so we chose  $\omega_{1,2,3}$  such that  $\Delta_1 = 0$ ,  $\Delta_2 = 40$ , and  $\Delta_3 = 80$ . Using this information as input we study the requirements for discrimination of the orderings following a similar approach to Ref. [26].

In brief, let’s assume that the observed rates  $N_{\gamma}^{\text{obs}}(\omega_i)$  for  $i = 1, 2, 3$  are those expected for some values of the oscillation parameters and some normalization rate  $N_{\text{norm}}$  for some ordering  $O_{\text{true}}$ . Notice that for simplicity we assume the true normalization to be the same for the three frequencies. We build the likelihood  $\mathcal{L}$  function for that data to be described within a given ordering “O” as

$$\chi_{\text{RENP},O}^2 = -2 \log(\mathcal{L}_O^{\text{RENP}}) = 2 \min_{\theta \in O} \left[ \sum_{i=1}^3 N_{\gamma}^{\text{exp}}(\omega_i; \theta, O) - N_{\gamma}^{\text{obs}}(\omega_i) - N_{\gamma}^{\text{obs}}(\omega_i) \log \left( \frac{N_{\gamma}^{\text{exp}}(\omega_i; \theta, O)}{N_{\gamma}^{\text{obs}}(\omega_i)} \right) \right], \quad (31)$$

where  $N_{\gamma}^{\text{exp}}(\omega_i; \theta, O)$  is the number of expected RENP events with frequency  $\omega_i$  for parameters  $\theta$  (we label  $\theta$  a given set of values for the oscillation parameters and normalization) and for the ordering “O”. We then we define the test statistics  $T$  as

$$T = \chi_{\text{RENP},\text{IO}}^2 - \chi_{\text{RENP},\text{NO}}^2. \quad (32)$$

To determine the probability distribution of  $T$  we generate pseudo experiments Poisson distributed about  $N_{\gamma}^{\text{obs}}(\omega_i)$  and for each of them we compute the value of  $T$ . We show in Fig.4 as example the distribution for the case in



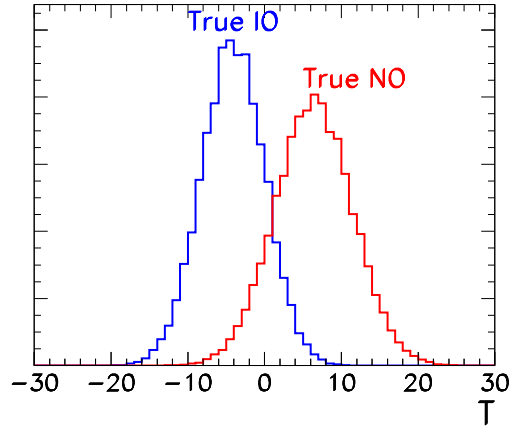


FIG. 4: Probability distribution for the  $T$  test statistics in Eq.(32) for events generated about  $N_{\gamma}^{\text{obs}}(\omega_i)$  as expected for Xe with  $\theta_{\text{true}}$  corresponding to the best fit values and  $m_0 = 0.01$  eV and  $N_{\text{norm}} = 3000$ . The blue (red) histogram correspond to  $O_{\text{true}}=\text{IO}$  (NO).

which  $N_{\gamma}^{\text{obs}}(\omega_i)$  are those expected for Xe with  $\theta_{\text{true}}$  corresponding to the best fit values and  $m_0 = 0.01$  eV and  $N_{\text{norm}} = 3000$ . The blue (red) histogram corresponds  $O_{\text{true}}=\text{IO}$  (NO), *i.e.* they are the distributions  $p(T, \text{IO})$  and  $p(T, \text{NO})$  respectively. As expected  $p(T, \text{NO})$  is peaked at positive values of  $T$  (since in this case  $\chi_{\text{REN}, \text{IO}}^2$  is most likely larger than  $\chi_{\text{REN}, \text{NO}}^2$ ) while the opposite holds for  $p(T, \text{IO})$ . As  $N_{\text{norm}}$  increases the distributions become more sharply peaked, so the overlap between them decreases.

The question we want to address is for what minimum value of  $N_{\text{norm}}$  the overlap is small enough so we can discriminate against the wrong ordering at a given CL,  $1 - \alpha$ . In order to quantify this, we make use of the condition that the *median sensitivity* is smaller than  $\alpha$ . This condition imposes that the median of the distribution with the right ordering (ie the value of  $T_c$  for which 50% of the pseudo-experiments have  $T > T_c$  and 50% have  $T < T_c$ ) has a probability smaller than  $\alpha$ , in the distribution of the wrong ordering. This is, for true NO we need to find  $N_{\text{norm}}$  for which

$$\int_{T_c^{\text{NO}}}^{\infty} p(T, \text{IO}) \leq \alpha. \quad (33)$$

Conversely for true IO we need to find  $N_{\text{norm}}$  for which

$$\int_{-\infty}^{T_c^{\text{IO}}} p(T, \text{NO}) \leq \alpha. \quad (34)$$

The result of this exercise is shown in Fig. 5. In the figure we plot the minimum value of  $N_{\text{norm}}$  for which the median sensitivity to discriminate between orderings is 99% CL as a function of the neutrino mass scale  $m_0$ . In the left (right) panel the true ordering is NO (IO). The full lines are obtained keeping the oscillation parameters fixed to the best fit values of the present oscillation analysis given in Eq. (2). The dashed lines include the effect of the present uncertainty on the oscillation parameters. In doing so the oscillation parameters are minimized over within the present allowed ranges of the global oscillation analysis in Ref. [7]. In order to include this effect we add to  $\chi_{\text{REN}}^2$  a gaussian bias for each of the oscillation parameters with central value and  $1\sigma$  error given in Eq. (2). As seen in the figure, the inclusion of this uncertainty makes the minimum required  $N_{\text{norm}}$  larger by a factor  $\mathcal{O}(1.5-2.5)$ . The results are also shown for the two atomic targets considered, Xe (lower blue curves) and Yb (higher red curves). In the figure we also see that for  $m_0 \lesssim 0.03$  the result is independent of  $m_0$  while for heavier neutrino mass scales, the minimum  $N_{\text{norm}}$  required grows with  $m_0$  because the sample values of  $I(\omega_i)$  are lower as  $m_0$  increases. For the same reason the required  $N_{\text{norm}}$  is always larger for true IO than for true NO.

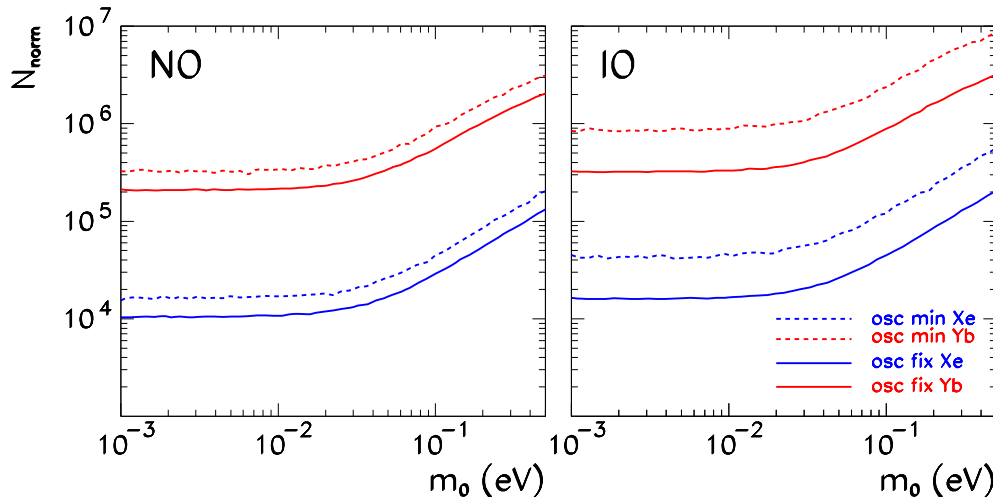


FIG. 5: Required value of the rate normalization factor in Eq.(26) for which the median sensitivity is better than 99% CL assuming that the true ordering is NO (left panel) and IO (right panel). In each panel the two upper (lower) curves correspond to atomic target of Yb (Xe). In the full lines the oscillation parameters are kept fixed to their best fit values given in Eq. (2). In the dashed lines they are minimized within the present allowed ranges of the global oscillation analysis in Ref. [7] (see text for details).

#### IV. SUMMARY AND OUTLOOK

In this work we have quantified the potential of macrocoherent atomic de-excitation via radiative emission of neutrino pairs as a probe of the neutrino mass spectrum. In particular we have evaluated the requirements for statistical determination of the most immediate unknowns of the neutrino spectrum: the neutrino mass scale and the mass ordering. In order to do so we have devised a minimum set of measurements and the associated statistical tests, capable of determining those neutrino properties in an idealized background free environment. We have considered two possible atomic targets whose lowest levels verify the conditions for RENP de-excitation: Xe and Yb.

Our results are summarized in Figs. 2 and 5. Figure 2 displays the required value of the rate normalization factors in Eq.(26) for the determination of the lightest neutrino mass  $m_0$  with  $3\sigma$  CL and given precision (1,10,50%). Figure 5 contains the corresponding results for the ordering determination at 99% CL.

Our results are sobering. Regardless of the particular behaviour of the curves in the figures we find that even under the ideal conditions assumed here, the required normalization for the  $3\sigma$  determination of  $m_0$  with accuracy better than 50% implies experimental live times of the order of days to years for each frequency for a target of volume of order  $100 \text{ cm}^3$  containing about  $10^{21}$  atoms per cubic centimeter in a totally coherent state with maximum value of the electric field in the target ( $\langle \eta_\omega \rangle \sim \mathcal{O}(1)$ ). Also comparing the results in Figs.2 and 5 we find that in order to discriminate between the mass orderings at 99% CL one needs similar target coherence and running time conditions to those required for the determination of the mass scale at  $3\sigma$ . Such conditions seem to be, as of today, way beyond the reach of our current technology.

#### Acknowledgments

M.C.G-G and N.S are supported by USA-NSF grant PHY-13-16617 and by FP7 ITN INVISIBLES (Marie Curie Actions PITN-GA-2011-289442). M.C.G-G also acknowledges support by grants 2014-SGR-104 and by FPA2013-46570 and consolidator-ingenio 2010 program CSD-2008-0037. J.J.G-C is also supported by the following agencies and institutions: the European Research Council (ERC) under the Advanced Grant 339787-NEXT; the Ministerio de Economía y Competitividad of Spain under grants CONSOLIDER-Ingenio 2010 CSD2008-0037 (CUP), FPA2009-

13697-C04 and FIS2012-37947-C04.

- 
- [1] B. Pontecorvo, Sov. Phys. JETP **26**, 984 (1968).
  - [2] V. N. Gribov and B. Pontecorvo, Phys. Lett. **B28**, 493 (1969).
  - [3] M. C. Gonzalez-Garcia and M. Maltoni, Phys. Rept. **460**, 1 (2008), 0704.1800.
  - [4] Z. Maki, M. Nakagawa, and S. Sakata, Prog. Theor. Phys. **28**, 870 (1962).
  - [5] M. Kobayashi and T. Maskawa, Prog. Theor. Phys. **49**, 652 (1973).
  - [6] J. Beringer et al. (Particle Data Group), Phys. Rev. **D86**, 010001 (2012).
  - [7] M. C. Gonzalez-Garcia, M. Maltoni, and T. Schwetz, JHEP **11**, 052 (2014), 1409.5439.
  - [8] P. Adamson et al. (MINOS), Phys. Rev. Lett. **112**, 191801 (2014), 1403.0867.
  - [9] K. Abe et al. (T2K), Phys. Rev. **D91**, 072010 (2015), 1502.01550.
  - [10] R. B. Patterson (NOvA) (2012), [Nucl. Phys. Proc. Suppl.235-236,151(2013)], 1209.0716.
  - [11] K. Abe et al. (Hyper-Kamiokande Proto-Collaboration), PTEP **2015**, 053C02 (2015), 1502.05199.
  - [12] M. Bass et al. (LBNE), Phys. Rev. **D91**, 052015 (2015), 1311.0212.
  - [13] J. Bonn et al., Nucl. Phys. Proc. Suppl. **91**, 273 (2001).
  - [14] V. M. Lobashev et al., Nucl. Phys. Proc. Suppl. **91**, 280 (2001), 19th International Conference on Neutrino Physics and Astrophysics - Neutrino 2000, Sudbury, Ontario, Canada, 16-21 Jun 2000.
  - [15] A. Osipowicz et al. (KATRIN) (2001), hep-ex/0109033.
  - [16] J. J. Gomez-Cadenas, J. Martin-Albo, M. Mezzetto, F. Monrabal, and M. Sorel, Riv. Nuovo Cim. **35**, 29 (2012), 1109.5515.
  - [17] C. Macolino (GERDA), Mod. Phys. Lett. **A29**, 1430001 (2014), 1312.0562.
  - [18] A. Gando et al. (KamLAND-Zen), Phys. Rev. Lett. **110**, 062502 (2013), 1211.3863.
  - [19] J. B. Albert et al. (EXO-200), Phys. Rev. **C89**, 015502 (2014), 1306.6106.
  - [20] K. Alfonso et al. (CUORE) (2015), 1504.02454.
  - [21] M. Yoshimura, Phys. Lett. **B699**, 123 (2011), 1101.2749.
  - [22] A. Fukumi, S. Kuma, Y. Miyamoto, K. Nakajima, I. Nakano, et al., PTEP **2012**, 04D002 (2012), 1211.4904.
  - [23] D. N. Dinh, S. T. Petcov, N. Sasao, M. Tanaka, and M. Yoshimura, Phys. Lett. **B719**, 154 (2013), 1209.4808.
  - [24] M. Yoshimura, N. Sasao, and M. Tanaka, Phys. Rev. **A86**, 013812 (2012), 1203.5394.
  - [25] N. I. of Standards and T. (NIST), <http://www.nist.gov/pml/data/handbook/index.cfm>.
  - [26] M. Blennow, P. Coloma, P. Huber, and T. Schwetz, JHEP **03**, 028 (2014), 1311.1822.